

Direct Measurement of Beam-Induced Fields in Accelerating Structures

H. Figueroa,^(a) W. Gai, R. Konecny, J. Norem, A. Ruggiero,^(b) P. Schoessow, and J. Simpson

Argonne National Laboratory, Argonne, Illinois 60439

(Received 22 February 1988)

We have developed a new method for measuring the electromagnetic fields (wake fields) induced in high-frequency accelerating devices by intense relativistic electron bunches. These fields are probed by a second collinear electron bunch which follows the primary bunch at a variable delay. Initial results for several iris-loaded rf structure geometries are presented. This technique is expected to be important for the study of new acceleration methods such as the plasma wake-field accelerator. Another possible application is the measurement of parasitic wakes in conventional accelerator components.

PACS numbers: 41.80.Ee, 07.77.+p, 29.15.-n

The need for higher accelerating gradients to decrease the size, cost, and complexity of future linear colliders for particle-physics research has motivated the development of new ideas for charged-particle acceleration. In particular, many so-called wake-field schemes have been proposed¹⁻³ in which an intense, low-energy beam excites electric fields in a cavity or medium which are then used to accelerate a second, less intense beam to high energies. In addition, even for accelerators not based on the wake-field principle, it is important to understand the effects of transverse wake fields induced in beam-line components as contributing to beam instabilities and emittance growth.⁴

To understand the physical mechanism of the wake field, consider the cavity shown in Fig. 1. The relevant parameters are the dimensions of the individual cavity cells a , b , and g , the number of cells N , the rms bunch length σ_D and charge Q_D of the driver bunch, and the distance the test particle lags behind the driver, $z = c\tau$, where τ is the relative delay and the particle velocity $\approx c$. The beam excites both longitudinal (E_z) and transverse fields (E_r and H_ϕ). The longitudinal wake potential, which is of particular interest, can be defined as the energy change of the test particle as it passes through the structure.⁵ This can be expanded as the sum of cavity modes. Define

$$U(z) = e \int_0^{Ng} E_z(z', (z'+z)/c) dz' = \sum_n W_n \cos K_n z,$$

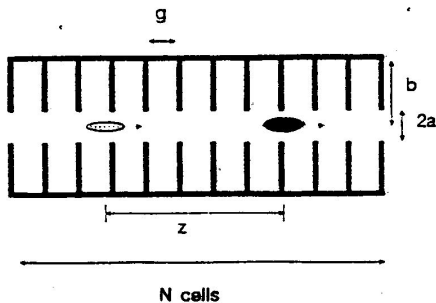


FIG. 1. Schematic of the test cavity geometry.

where a generic mode is described by the amplitude W_n and the wave number K_n , with the total wake potential given by the sum of all modes. We shall denote the parameters of the fundamental mode by W_0 and K_0 . For the case $a=0$ and $\sigma_D=0$, K_n and W_n can be found analytically with $K_n = j_{0n}/b$, where j_{0n} is the n th zero of the Bessel function $J_0(x)$. For the case of finite aperture $a > 0$, the wake potential must be found numerically. For a bunch with longitudinal charge-density distribution $f(z)$, the wake potential for a test particle at location z is

$$U(z) = \sum_n W_n \int_z^\infty f(z') \cos K_n(z'-z) dz'.$$

In particular, for a Gaussian distribution with rms length σ_D and a particle at a distance $z \gg \sigma_D$ from the center of the driver,

$$U(z) = \sum_n W_n \exp(-K_n^2 \sigma_D^2 / 2) \cos K_n z.$$

In order to study wake-field effects, we designed and constructed the Advanced Accelerator Test Facility at Argonne National Laboratory. The facility allows direct measurement of the longitudinal and transverse wake fields of an intense electron driver beam through their effects on a low-intensity "witness" beam.

The layout of the test facility is shown in Fig. 2. 21.4-MeV electrons from the Argonne chemistry division L-band linac are transported to the entrance of the facility where about 25% of the beam strikes a small carbon target and is degraded in energy to 15 MeV to produce a secondary electron beam several orders of magnitude less intense than the primary beam. The first dipole splits the primary driver beam and the low-energy witness beam which then pass through their respective beam lines, to be recombined symmetrically before the test section.

The length of the low-energy line is mechanically adjustable so that the delay of the witness beam relative to the driver beam can be varied. Following the test section is a double-focusing spectrometer, which allows measurement of both energy and transverse position changes of either beam.

Measurements of the beam position in the facility and

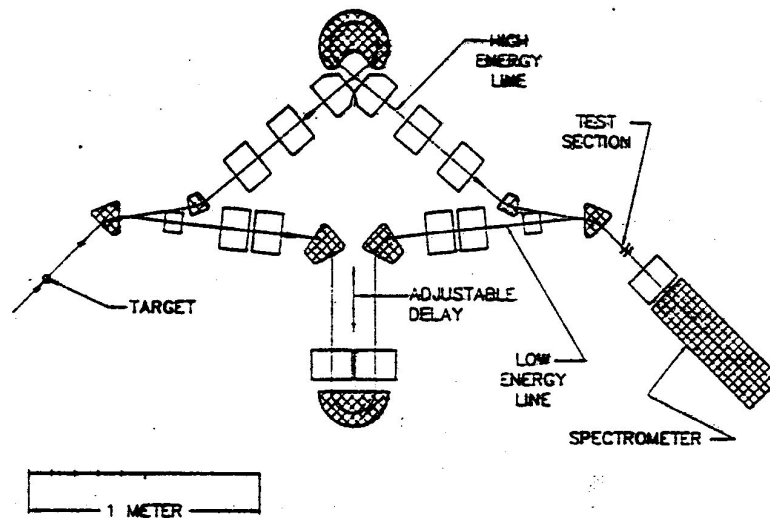


FIG. 2. Plan view of the Advanced Accelerator Test Facility. Beam-line magnets are dipoles (cross hatched) or quadrupoles (open).

at the spectrometer focal plane are made with use of phosphorescent screens. Conventional closed-circuit television cameras are used to detect the light from the beam striking the phosphor, with the exception of the witness beam at the spectrometer, where, because of the small beam current, a camera equipped with a microchannel-plate image intensifier must be used. The video signals were digitized with a Data Translation model DT-2803 frame grabber interfaced to an IBM PC/XT computer and stored on disk for offline analysis.

A Hamamatsu model C1587 streak camera was used to measure the beam pulse length using the Cherenkov radiation pulse produced by the driver beam on a Xe-filled quartz cell. This was determined to be 25 ± 5 ps FWHM for the data presented here. The average beam current was measured from the current deposited in the spectrometer magnet which is grounded through a picoammeter and thus acts as a Faraday cup. For these data the beam current was $\approx 2-3$ nC/pulse, with small ($\approx 5\%$) point-to-point fluctuations over the duration of a cavity scan.

The data for each cavity were obtained by our changing the witness-beam delay by a fixed amount, then acquiring a frame of the witness-beam spot. At the same time, the driver current was also measured and recorded. The procedure was repeated until several cycles of the

wake field were measured.

We have measured three cavities constructed from aluminum washers inserted into the beam pipe of the test section. The dimensions were chosen to study the wake-field effect for 5-10-GHz structure and also the wake-field dependence on g and a/b . The experimental conditions are given in Table I.

Conversions from pixels to millimeters were obtained by our digitizing a scale inscribed on the focal-plane phosphor. The energy calibration was then found from the calculated dispersion function ($\eta = 0.568 \pm 0.007$ m) of the spectrometer to be 10.4 keV/pixel. The transverse (nonbend view) resolution was also measured to be 0.75 mm/pixel.

The experimental results for longitudinal wake fields in these cavities are shown in Figs. 3-5, where the shift in energy of the witness-beam centroid as a function of

TABLE I. Experimental conditions.

Cavity	b (cm)	a (cm)	g (cm)	$\sigma_p = \sigma_w$ (mm)	Q_D (nC)	N
1	1.95	0.63	0.63	4	3.1	60
2	1.95	0.63	0.32	4	2.31	103
3	1.25	0.63	0.32	4	2.22	100

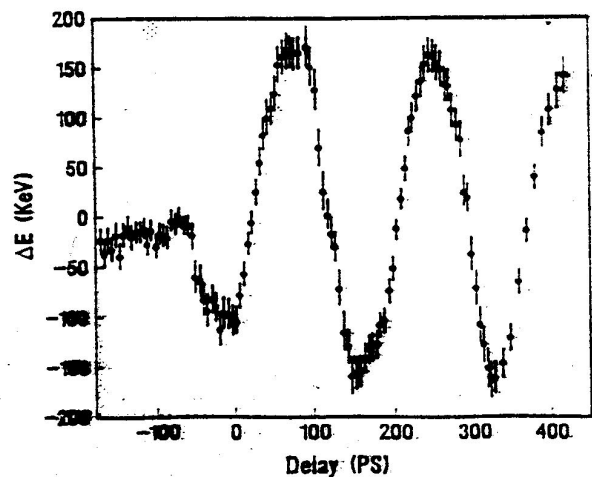


FIG. 3. Measured longitudinal wake potential for cavity 1.

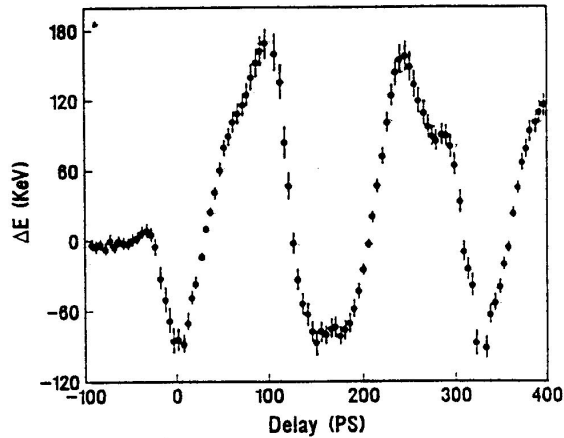


FIG. 4. Measured longitudinal wake potential for cavity 2.

delay is shown for each of the three cavity geometries. The error on each point reflects the statistical uncertainty in the centroid determination, and the pulse-to-pulse driver charge fluctuations.

For negative delays, the witness precedes the driver through the cavity and thus by causality is unaffected. As the delay is increased, and the witness bunch overlaps the driver, it begins to lose energy as it feels the retarding field induced by the driver bunch. As the delay increases, the witness beam starts to gain energy. Since the energy change of the witness beam measures the wake-field amplitude, the wake field inside the driver bunch is smaller than that behind the bunch. At still larger delays, the energy modulation of the witness beam is nearly sinusoidal.

The data for cavity 1 (Fig. 3) show a fundamental wake amplitude of about 200 keV with a period of 180 ps. Small-amplitude higher-order modes are also excited which are superimposed on the fundamental. The driver and witness bunches are sufficiently long that the fundamental mode (W_0 and K_0) predominates in the observed wake fields.

For cavity 2, the experimental results show the same features as cavity 1. The data also exhibit a small higher-order mode contribution, the effects of which are clearly seen at 100- and 180-ps delay. The kink at 280 ps is not due to the higher modes, but is an experimental artifact possibly due to a binding in the motion of the delay (trombone) assembly.

The results for cavity 3 are shown in Fig. 5. As expected, the wake-field amplitude is larger than for cavities 1 and 2, because the wake-field strength should be inversely proportional to the diameter of the cavity.

For comparison with Fig. 3, we have calculated the longitudinal wake potential numerically using the TBCI code⁶ for the cavity-1 geometry and beam intensity (Fig. 6). The code computes the longitudinal wake potential for a Gaussian-shaped driver bunch and a zero-length

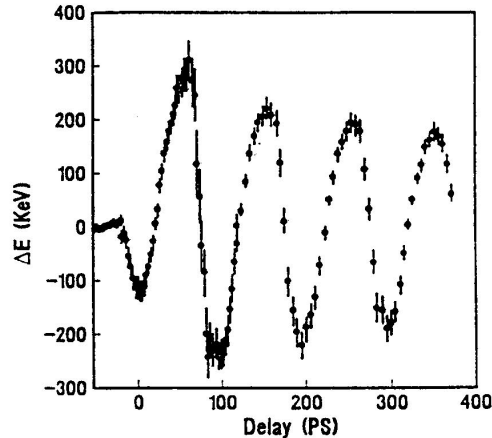


FIG. 5. Measured longitudinal wake potential for cavity 3.

witness bunch. Accordingly, we have smeared the TBCI result by a Gaussian resolution function with rms width $\sigma_w = \sigma_D$ to account for the effect of nonzero witness-bunch length. We find that the computed wake field gives a reasonable agreement with experimental data in both amplitude and frequency.

We have also observed transverse wakes in this experiment. If the driving beam passes through the cavity off axis it excites higher-order azimuthal modes, principally the TM_{110} mode. Figure 7 shows examples of the transverse deflection (nonbend view centroid motion) of the witness beam versus delay for cavities 2 and 3, with the driving beam displaced ≈ 1 mm from the cavity axis. For cavity 2, it shows a 120-ps period oscillation, compared with the fundamental frequency of 180 ps. This is identified as the TM_{110} mode as predicted by a simple pill-box cavity model.⁷ (Cavity 3 shows the same feature as cavity 2, but with a 70-ps period.) This

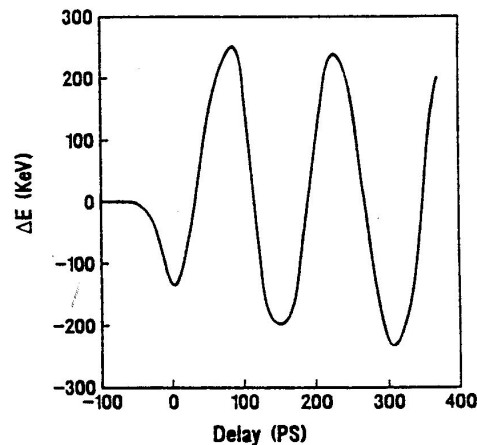


FIG. 6. Longitudinal wake in cavity 1 as computed by the program TBCI.

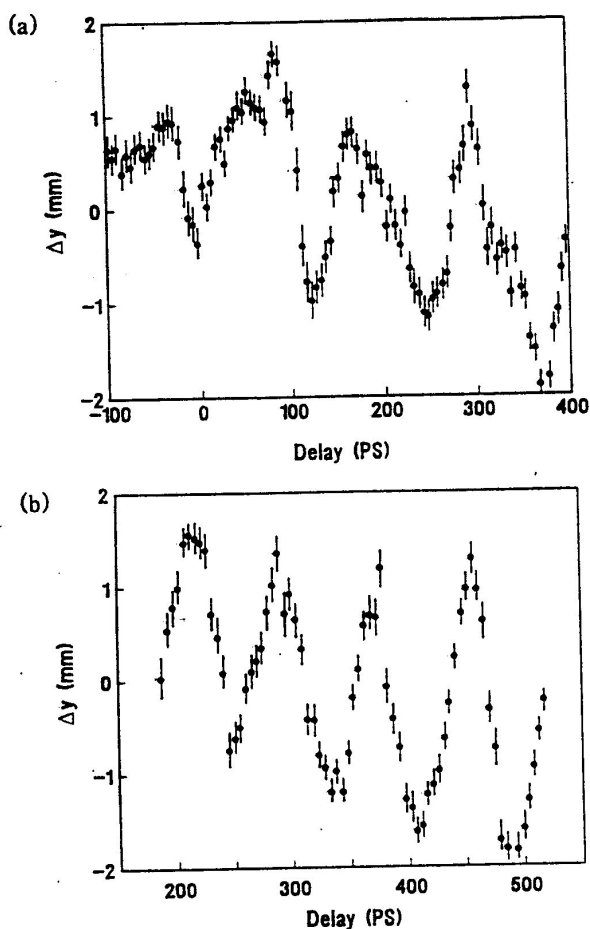


FIG. 7. (a) Cavity-2 transverse wake and (b) cavity-3 transverse wake.

transverse mode is of interest as a source of beam breakup in linear accelerators.⁴

To summarize, we have designed and constructed a

unique facility to measure longitudinal and transverse wake-field effects for high-frequency accelerating devices. The technique is applicable for the study both of novel acceleration methods (for example, plasma-wake-field acceleration schemes⁸), and of parasitic wake-field effects in conventional rf structures.

The authors gratefully acknowledge the assistance of J. MacLachlan, J. Rosenzweig, B. Cole, and C. Jonah. The authors would also like to thank D. Cline for his continuing encouragement of this work.

This work is supported by the U.S. Department of Energy, Division of High Energy Physics, Contract No. W-31-109-ENG-38.

^(a)Current address: University of Southern California, Los Angeles, CA 90089.

^(b)Current address: Brookhaven National Laboratory, Upton, NY 11973.

¹A. Ruggiero, P. Schoessow, and J. Simpson, in *Advanced Accelerator Concepts*, edited by F. Mills, AIP Conference Proceedings No. 156 (American Institute of Physics, New York, 1987), p. 247.

²P. Chen and J. Dawson, in *Laser Acceleration of Particles*, edited by C. Joshi and T. Katsouleas, AIP Conference Proceedings No. 130 (American Institute of Physics, New York, 1986) p. 201.

³W. Bialowens *et al.*, in Ref. 1, p. 266.

⁴P. Wilson, in *Physics of High Energy Particle Accelerators*, edited by R. Carrigan, F. Huson, and M. Month, AIP Conference Proceedings No. 87 (American Institute of Physics, New York, 1982), p. 450.

⁵K. Bane *et al.*, in *Physics of High Energy Particle Accelerators*, edited by M. Month, P. Dahl, and M. Dienes, AIP Conference Proceedings No. 127 (American Institute of Physics, New York, 1984), p. 876.

⁶T. Weiland, *Part. Accel.* 15, 245 (1984).

⁷W. Gai, private communication.

⁸J. Rosenzweig *et al.*, *Bull. Am. Phys. Soc.* 32, 1787 (1987).